

Programmable Kondo Effect Formed by Landau Levels

Hong Chen,¹ Yun Chen,¹ Rui Wang,^{1,2,3,*} and Baigeng Wang^{1,2,†}

¹National Laboratory of Solid State Microstructures and Department of Physics, Nanjing University, Nanjing 210093, China

²Collaborative Innovation Center of Advanced Microstructures, Nanjing University, Nanjing 210093, China

³Hefei National Laboratory, Hefei 230088, People's Republic of China

Nanobubbles wield significant influence over the electronic properties of 2D materials, showing diverse applications ranging from flexible devices to strain sensors. Here, we reveal that a strongly-correlated phenomenon, *i.e.*, Kondo resonance, naturally takes place as an intrinsic property of graphene nanobubbles. The localized strain within the nanobubbles engenders pseudo magnetic fields, driving Landau quantization with degenerate Landau orbits. Under the Coulomb repulsion, the Landau orbits form an effective $SU(N)$ pseudospin intricately coupled to the bath via exchange interaction. This leads to novel Kondo behaviors with a new flavor screening mechanism. The resonance here exhibits an unparalleled tunability via strain engineering, establishing a versatile platform for exploring novel correlated phenomena beyond the scope of conventional Kondo systems.

Introduction.— The Kondo effect stands as a cornerstone in condensed matter physics [1, 2], sparking pivotal developments across diverse fields, ranging from impurity physics [3] to quantum transport [4, 5]. Its essence lies in the presence of local degenerate quantum states (Fig.1(a)) [6], typically realized through spin states in dilute magnetic alloys [7] or quantum dot junctions [8, 9]. The spin-exchange coupling with the host environment then plays a critical role in driving the many-body resonance, ultimately giving rise to the formation of Kondo singlet.

Manipulating the Kondo resonance, particularly its underlying symmetry, poses significant challenges [10], as it is dictated by intrinsic properties of the underlying material, such as the degeneracy N of the local quantum states. For example, extending the $SU(2)$ Kondo model to $SU(3)$ or $SU(4)$ necessitates intentionally designed, intricate mesoscopic structures [11], including carbon nanotubes [12–14] and vertical quantum dots [15]. It seems unlikely to realize the $SU(N)$ model with tunable N in a single setup. Introducing highly efficient tuning knobs, such as N , to Kondo resonance is of crucial importance [10]. Not only does this guarantee a variety of tunable Kondo phenomena [16–19], but also lays the foundation for realizing controllable Kondo lattices that host novel correlated physics [20–24].

In this Letter, we unveil a novel form of Kondo phenomena characterized by exceptional tunability and a fundamentally distinct mechanism. Our focus here is specifically on Kondo behaviors emergent from nanobubbles [25–29] located on the surfaces of two-dimensional (2D) materials [30–33], particularly graphene sheets. Graphene nanobubbles (GNB) represent smooth, dome-shaped deformations that induce localized strain [34, 35] (Fig.1(c)). The strain generates pseudo magnetic fields within the bubble region [36, 37], giving rise to a Landau level (LL) [38, 39] with N degenerate orbits. These orbits carry the “flavor” quantum number, j , and are termed Landau sites (LSs) [40] (Fig.1(b)). Notably, the LSs provide the key ingredient for Kondo resonance, *i.e.*, the degenerate quantum states, akin to the spin states (Fig.1(a)). Moreover, the GNB is not isolated but coupled to the thermal bath, as illustrated by the bilayer model in Fig.1(c). This coupling manifests in low-energy as the hybridization between

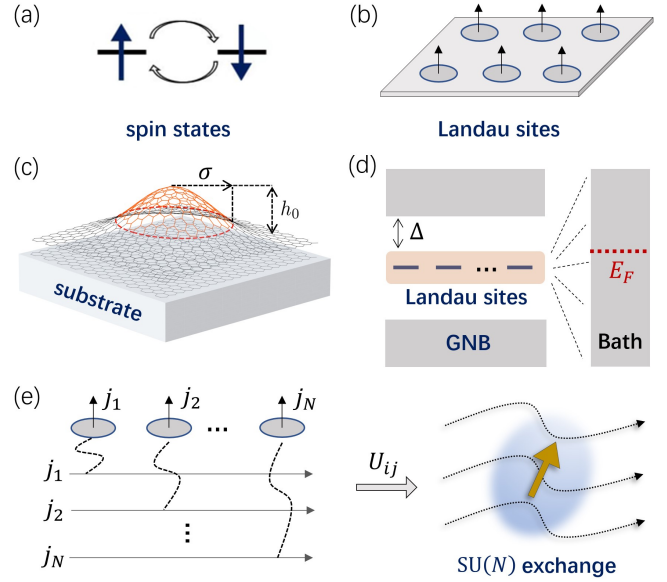


FIG. 1. (a) The degenerate spin states constitute the key ingredient for Kondo effect. (b) The schematic plot of degenerate LSs characterized by flavor, j . (c) Plot of a bilayer graphene with a GNB on the top layer. (d) The LSs are separated by a gap from the higher energy states of the GNB, and are effectively coupled to the bath. (e) The flavor is conserved in the coupling, and an $SU(N)$ pseudospin emerges from the LSs with considering the Coulomb repulsion, leading to $SU(N)$ Kondo resonance.

the LSs and the bath (Fig.1(d)). Intriguingly, flavor conservation is maintained, and each LS is hybridized with an effective 1D bath mode bearing the same flavor (Fig.1(e)), resembling the Anderson impurity model [7]. Further considering the Coulomb interaction, an effective $SU(N)$ pseudospin then emerges, generating the $SU(N)$ Kondo resonance (Fig.1(e)).

The GNBs have been extensively studied and demonstrated to be programmable [27], owing to their high tunability. The N -degeneracy here can be manipulated by strain engineering. Thus, $SU(N)$ Kondo models with successively tunable N are realized in a single platform. Moreover, the number and spatial distribution of GNBs, alongside the Fermi energy of the

bath, can all be well controlled. This unprecedented tunability establishes a flexible experimental framework for investigating Kondo and heavy fermion physics with new mechanisms beyond conventional setups.

Landau sites in GNBs.— We first analyze the strain effect in a graphene monolayer. The strain induces local lattice distortion. The three nearest neighbor lattice vectors δ_n , with $n = 1, 2, 3$, are modulated to $\mathbf{d}_n = \delta_n + \bar{u}\delta_n$, where \bar{u} is the strain tensor defined by $u_{ij} = (\partial_i u_j + \partial_j u_i + \partial_i z \partial_j z)/2$, with $i, j = 1, 2$. Here, $\mathbf{u} = (u_1, u_2)$ and z are respectively the in-plane and out-of-plane deformation. The three nearest neighbor hoppings are accordingly modulated, *i.e.*, $t_n = t_0 e^{-\beta(|\mathbf{d}_n|/a-1)}$, where t_0 is the original hopping and $\beta = 3.37$ is used [41, 42]. Consequently, the kinetic energy is modified at the \mathbf{K}^\pm valley, as if the Dirac fermions were coupled to a pseudo gauge field $\mathbf{A}(\mathbf{r})$, which satisfies $A_x(\mathbf{r}) - iA_y(\mathbf{r}) = \sum_n (t_n - t_0) e^{i\mathbf{K}^\pm \cdot \delta_n}$ [43]. The pseudo magnetic field, $B(\mathbf{r}) = \nabla \times \mathbf{A}(\mathbf{r})$, is known to generate Landau quantization [43, 44]. For example, in the case of triaxial strain with $\mathbf{u} \propto (2xy, x^2 - y^2)$, the corresponding $B(\mathbf{r})$ is uniform but opposite for the two valleys (B and $-B$ for \mathbf{K}^+ and \mathbf{K}^- respectively, and the flux $\Phi > 0$ is assumed). LLs are then formed for both valleys with $E_n = \text{sign}(n)v_F\sqrt{2|n|B}$ ($n = 0, \pm 1, \dots$).

In addition to the triaxial strain, a more natural description of GNBs is given by the out-of-plane Gaussian deformation [45, 46], $z(\mathbf{r}) = h_0 e^{-r^2/2\sigma^2}$, where σ and h_0 are respectively the radius and the height of the GNB (Fig.1(c)). In this case, the pseudo magnetic field is non-uniform [47]. Nevertheless, the averaged flux, $\bar{\Phi} = \int d\mathbf{r} B(\mathbf{r})$, becomes nonzero for $N = |N_B - N_A| \neq 0$, where N_A and N_B are the number of A and B sublattices in the strained area. This leads to zero-energy LL with degeneracy N , as ensured by the Lieb-Sutherland theorem [48–50]. N can be as small as 2 and successively tuned via strain engineering of the GNB.

We plot the hopping amplitude t_n for the Gaussian deformation in Fig.2(a). t_n decreases from t_0 at the bubble center, and decays to nearly vanishing values before it further increases up to t_0 at larger r . Thus, a strained subsystem (denoted by Ω) is automatically separated and weakly coupled to the rest of the graphene flake. Ω is described by $H_{\text{sys}} = -\sum_{\mathbf{r} \in \Omega, n} t_n \psi^\dagger(\mathbf{r})\psi(\mathbf{r} + \delta_n) + \text{h.c.}$, where $\psi(\mathbf{r})$ is the annihilation operators of electrons at \mathbf{r} . The corresponding energy spectrum is obtained and shown by Fig.2(b). For $N = |N_B - N_A|$, we always find N degenerate zero energy modes, in consistence with Lieb-Sutherland theorem. Notably, the zero modes are isolated from the higher energy states by a significant gap Δ . For $N = 2$ and the total site number ~ 100 , $\Delta \sim 60 \text{meV} \simeq 696K$. Thus, the low-energy physics of the GNB is well captured by the zero modes.

For $N = 2$, the wavefunction distributions of the two zero modes are shown in Fig.2(c)-(d). Their analytic forms can be derived by solving the Liepmann-Schwinger equation describing the scattering of electrons by the non-uniform gauge potential $\mathbf{A}(\mathbf{r})$ [51]. In the symmetric gauge, the wave-

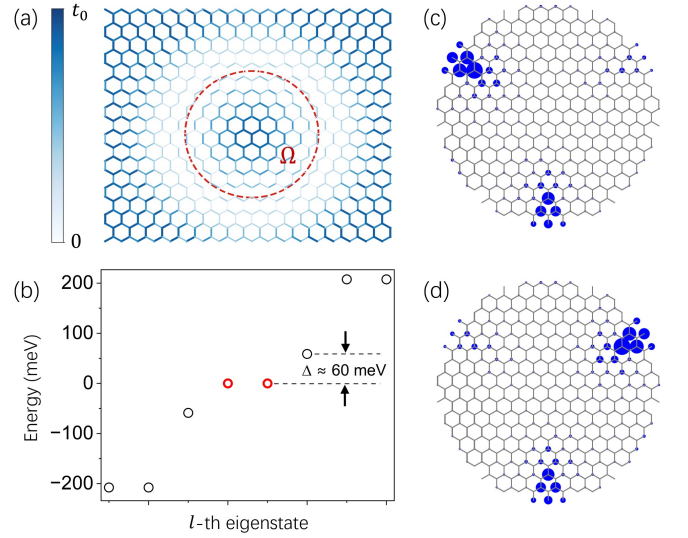


FIG. 2. (a) The hopping distribution t_n . The minima of t_n lie on the red sphere, which separates the strained GNB (Ω) from the rest, unstrained area. $N_A = 61$, $N_B = 63$ and $N = 2$ in Ω . (b) The low-energy spectrum of the GNB in (a). Two zero modes emerge denoted by the red circles, isolated by a gap Δ from the higher energy states. (c),(d) The spatial distribution of the wavefunction corresponding to the two zero modes.

functions $\Psi_m^{(\xi)}(\mathbf{r})$ are sublattice polarized, and characterized by the orbital angular momentum (OAM) m and the valley index $\xi = \pm$. For example, in the triaxial strain case with uniform B , $\Psi_m^{(\xi)}(\mathbf{r})$ is reduced to the typical Landau wavefunction, which, in the sublattice basis, reads as [47], $\Psi_m^{(\xi)}(\mathbf{r}) = [0, z_\xi^m (r/r_0)^{-N_\Phi}]^T$ with $m = 0, 1, \dots, N_\Phi$, where $N_\Phi = \bar{\Phi}/2\pi$ is the number of flux quanta, r_0 is a constant, and $z_\xi = y + i\xi x$ is the complex coordinate. $\Psi_m^{(\xi)}(\mathbf{r})$ is fully polarized as its component is nonzero only on B sublattice.

For convenience, we introduce the flavor, $j = (\xi, m)$ and represent the degenerate zero modes by $|j\rangle = d_j^\dagger |0\rangle$, where $|0\rangle$ denotes the vacuum, d_j^\dagger is the creation operator that satisfies, $\{d_j, d_{j'}^\dagger\} = \delta_{j,j'}$. These zero modes are known as LSs following the quantum Hall physics [40]. However, a key difference here is that their degeneracy is restricted to $N = |N_B - N_A|$.

Emergent $SU(N)$ Anderson model.— In realistic materials, the LSs in a GNB are inevitably subjected to many-body interactions, as well as hybridizations with the hosting environment. To better investigate these effects, we consider Bernal-stacked bilayer graphene with a GNB (Fig.1(c)). As illustrated by Fig.3(a), the GNB subsystem Ω is coupled to the bilayer environment ($\bar{\Omega}$).

We take into account the electron-electron interaction in the GNB [52], $H_{\text{int}} = \int d\mathbf{r} d\mathbf{r}' U(\mathbf{r} - \mathbf{r}') \psi^\dagger(\mathbf{r})\psi(\mathbf{r})\psi^\dagger(\mathbf{r}')\psi(\mathbf{r}')$, where $U(\mathbf{r} - \mathbf{r}')$ is short-ranged due to the strong screening in the bilayer [53]. For $U(\mathbf{r} - \mathbf{r}') = 0$, Ω exhibits LSs on the zeroth LL separated by an energy gap from the other states (Fig.2(b)). In the second-quantized form, they are formally

described by

$$H_d = \sum_{j=1}^N \epsilon_d d_j^\dagger d_j, \quad (1)$$

where $\epsilon_d = 0$. The density of states (DOS) of Ω is shown by the red curve in the inset to Fig.3(b). The zero-energy peak emerges due to the LSs.

The interaction H_{int} projected to the zeroth LL is cast into [47],

$$H_{\text{int}} = \sum_{i \neq j} U_{ij} d_i^\dagger d_i d_j^\dagger d_j, \quad (2)$$

where U_{ij} is the projected direct integral between the LSs with the flavors, $i = (\xi', m')$ and $j = (\xi, m)$. For the hardcore repulsion, U_{ij} is evaluated as [40], $U_{ij} = (m + m')! / 8\pi l_B 2^{m+m'} m! m'!$, where l_B is the magnetic length.

We then calculate the DOS of the environment $\bar{\Omega}$. The DOS appears almost the same as that of the pristine bilayer graphene (Fig.3(b)). This agreement maintains in low-energy, exhibiting a finite DOS around $\omega = 0$, as shown by the Supplemental Material. Thus, we arrive at a low-energy bath continuum occurring simultaneously with the zero-energy LSs (inset to Fig.3(b)).

To visualize the hybridization between the LSs and bath continuum, we diagonalize the total system for $U_{ij} = 0$. Comparing the energy spectrum in Fig.3(c) and Fig.2(b), it is found that the LSs are shifted away from $E = 0$. The shift becomes more and more significant with increasing the system-environment coupling (inset to Fig.3(c)). This clearly reveals that the LSs are hybridized with the bath (Fig.1(d)), a prerequisite for Kondo resonance. Since the Kondo resonance is quantitatively determined by the bath DOS around the Fermi energy [7], replacing Ω by the pristine graphene bilayer can facilitate our numerical calculations without altering the Kondo behaviors.

Analytically, the hybridization can be measured by the overlap, $V = \langle j | \phi_{\mathbf{k},B}^{(\xi)} \rangle$, where $|\phi_{\mathbf{k},B}^{(\xi)}\rangle$ is the Bloch wavefunction on B sublattice of the bilayer. Note that $\langle j | \phi_{\mathbf{k},A}^{(\xi)} \rangle$ vanishes because of the sublattice polarization. In the band basis, $|\phi_{\mathbf{k},B}^{(\xi)}\rangle$ is represented by, $|\phi_{\mathbf{k},B}^{(\xi)}\rangle = (-e^{-i2\xi\theta} |c_{\mathbf{k},+}^{(\xi)}\rangle + e^{i2\xi\theta} |c_{\mathbf{k},-}^{(\xi)}\rangle) / \sqrt{2}$, where $|c_{\mathbf{k},\pm}^{(\xi)}\rangle$ denotes the Bloch state of conduction/valance band electrons at valley ξ , and θ is the angle of \mathbf{k} . Expanding $|c_{\mathbf{k},\pm}^{(\xi)}\rangle$ by the OAMs, *i.e.*, $u_{\mathbf{k},\pm}^{(\xi)} \equiv \langle \mathbf{r} | c_{\mathbf{k},\pm}^{(\xi)} \rangle = \sum_m u_{k,m,\pm}^{(\xi)} e^{im\theta}$, the hybridization between the LSs and the conduction/valance electrons is then obtained as, $V_{\pm} = \mp \delta_{\xi\xi'} \delta_{m',m\xi-2\xi} v_{k,\xi,m'} / \sqrt{2}$, where $v_{k,\xi,m} = \int_0^\infty dr r^m (r/r_0)^{-N_\Phi} u_{k,m,\pm}^{(\xi)}(r)$.

Interestingly, two Kronecker-delta function occurs in V_{\pm} , enforcing the valley and the OAM conservation, a reflection of the fact that the lattice deformation is smooth in GNBS. Notably, the OAM quantum number is changed by 2 in the hybridization, as a result of the pseudospin(sublattice)-

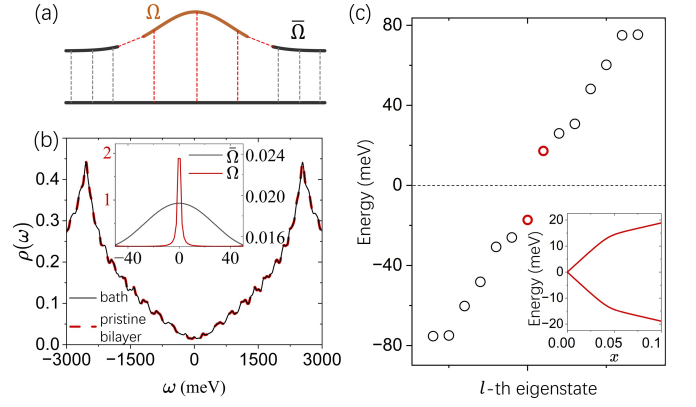


FIG. 3. (a) The sideview of the bilayer graphene with a GNB on the top layer. The subsystem Ω is coupled to the bilayer environment $\bar{\Omega}$ (b) The DOS of $\bar{\Omega}$ compared with that of pristine bilayer graphene. The inset shows the separate DOS of Ω and $\bar{\Omega}$ around $\omega = 0$. (c) The energy spectrum of the total system $\Omega + \bar{\Omega}$ with their couplings. The couplings (both intra- and inter-layer) are parameterized by $t = xt_0$, with $0 < x \ll 1$. The shifted LSs are highlighted by red, and $x = 0.1$ is used. The inset shows the shift with increasing x .

momentum locking intrinsic to the graphene bilayer [54]. In the second-quantized form, the above hybridization process is described by [47],

$$H_{\text{hyb}} = \int dk \sum_j v_{k,j} d_j^\dagger (-c_{k,j,+} + c_{k,j,-}), \quad (3)$$

where the c -fermions denote the operators of the bath electrons with shifted OAMs. Similarly, the bath Hamiltonian is reduced to the following low-energy theory,

$$H_{\text{bath}} = \int dk \sum_{j,n} (\epsilon_{k,n} - \mu) c_{k,j,n}^\dagger c_{k,j,n}, \quad (4)$$

where $\epsilon_{k,n} = nk^2/2m$, with $n = \pm$. We have also introduced the chemical potential μ of the bath, which can be tuned by gate voltage.

Further introducing effective fermionic operators in the energy representation that combine the conduction and valence bands [55, 56], *i.e.*, $\gamma_{\epsilon,j} = [-c_{\epsilon,j,+} + \theta(\epsilon) + c_{\epsilon,j,-} - \theta(-\epsilon)]/2$ and $\gamma_{\epsilon,j}^\dagger = [-c_{\epsilon,j,+}^\dagger + \theta(\epsilon) + c_{\epsilon,j,-}^\dagger - \theta(-\epsilon)]/2$, we finally arrive at,

$$H_{\text{bath}} = \sum_{j=1}^N \int_{-D}^D d\epsilon (\epsilon - \mu) \gamma_{\epsilon,j}^\dagger \gamma_{\epsilon,j}, \quad (5)$$

and

$$H_{\text{hyb}} = \sum_{j=1}^N \int_{-D}^D d\epsilon [h_j(\epsilon) d_j^\dagger \gamma_{\epsilon,j} + h.c.], \quad (6)$$

where D is the energy cutoff, $h_j(\epsilon) = |v_{\epsilon,j}|^2 \rho_{\bar{\Omega}}(\epsilon)$ is the broadening function with $\rho_{\bar{\Omega}}(\epsilon)$ being the bath DOS. Interestingly, Eq.(6) implies that the zero-energy LSs are only cou-

pled to the bath states with the same flavor j . Furthermore, Eq.(4) indicates that the bath states of flavor j are essentially fermionic modes exhibiting 1D momentum k . Thus, we reveal a hidden N -flavor 1D hybridization model underlying the GNB, as demonstrated by Fig.1(e).

Remarkably, Eq.(1)-(2) and Eq.(5)-(6) altogether constitute an emergent Anderson impurity model. The ‘‘impurity states’’ here have N different flavors, displaying the $SU(N)$ symmetry. This $SU(N)$ Anderson model, an intrinsic property of the GNB, is of high tunability. The flavor number N and the chemical potential μ offer two tuning knobs to explore unconventional Kondo phenomena.

Kondo effect formed by LSs.– We solve the emergent $SU(N)$ Anderson model using full density matrix (FDM) numerical renormalization group (NRG) [57]. For $N = 2$, the two LSs are characterized by the quantum number $(+, 0)$ and $(-, 0)$, and are subjected to the interaction $U_0 \equiv U_{(+,0),(-,0)} = 1/8\pi l_B$. The single-particle energy level of the LSs is shown by Fig.4(a). For $0 < \mu < U_0$, the singly occupied states are favored, resulting in the flavor pseudospin-1/2. The hybridization to the bath further generates the s - d exchange term, driving the GNB to the Kondo fixed point [7]. While for $\mu > U_0$, the s - d exchange coupling is absent and thus the Kondo resonance is turned off.

For $N = 3$, three LSs take place with the flavors, $j = (+, 0), (-, 0), (+, 1)$, which interact with each other via $U_{(+,0),(-,0)} = U_0$ and $U_{(+,1),(-,0)} = U_{(+,1),(+,0)} = U_0/2$. In this case, the LSs exhibit three single-particle energy levels (Fig.4(b)), *i.e.*, $-\mu, U_0/2 - \mu$, and $3U_0/2 - \mu$. In contrast to the $N = 2$ case, the $SU(3)$ model exhibits a transition between the electron- and hole-type Kondo resonance separated by the resonant scattering point (RSP). At the RSP with $\mu = U_0/2$, the ground state of the isolated LSs has six-fold degeneracy, as the three singly and three doubly occupied states display the same energy $-U_0/2$. Consequently, the charge fluctuation is sufficiently strong, producing a many-body ground state where all the six states are mixed. For $0 < \mu < U_0/2$, the three singly occupied states are favored, which act as an $SU(3)$ pseudospin interacting with the thermal bath. For $U_0/2 < \mu < 3U_0/2$, the ground state of the isolated LSs are doubly occupied, leaving a hole on the unoccupied LS. Interestingly, this leads to a hole-like $SU(3)$ spin, resulting in similar Kondo resonance with the $0 < \mu < U_0/2$ region.

We calculate the temperature-dependent thermodynamics of LSs with varying μ . The entropy of the LSs decreases monotonously to 0 with lowering T (Fig.4(c)). For $0 < \mu < U_0/2$ (upper panel), an entropy plateau occurs, reflecting the freezing of high-energy degrees of freedom with lowering the energy scale. In the specific heat, two peaks emerge accordingly. With increasing μ to the RSP (middle panel), the entropy plateau disappears, accompanied by the merging of the specific heat peaks. For larger μ (lower panel), the plateau and the two peaks appear again and become more and more significant, implying the formation of hole-type Kondo resonance at lower temperatures. We also calculate the local DOS

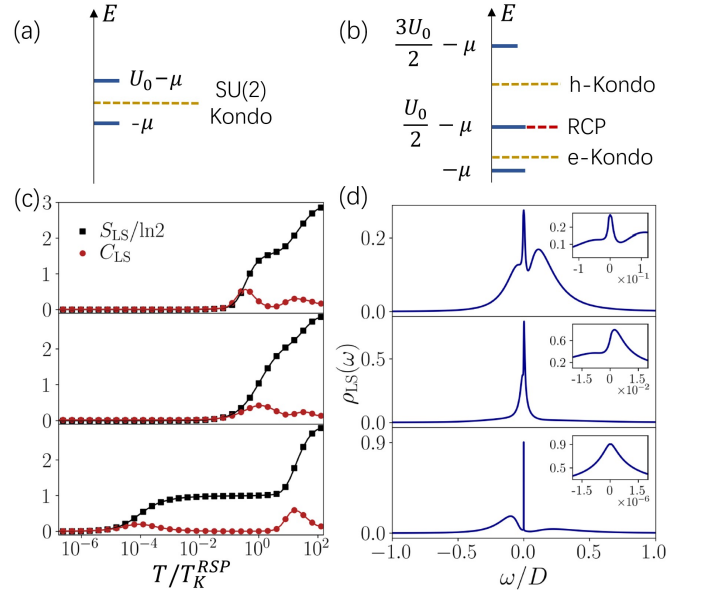


FIG. 4. The energy levels of the isolated LSs for $N = 2$ (a) and $N = 3$ (b). The Fermi energy of the bath is set to 0. (c) The temperature-dependent entropy and specific heat of the LSs for the $SU(3)$ model. T is normalized by the Kondo temperature at the RSP. (d) The LDOS of the LSs. $\mu/U_0 = 0.2, 0.5, 0.8$ from top to bottom in (c) and (d).

(LDOS) of the LSs (Fig.4(d)). With increasing μ , two resonant peaks at higher energies move towards the Kondo peak (at $\omega = 0$), merging with each other at the RSP. Then, they split for larger μ . The merging-resplitting behavior serves as a hallmark signature of the $SU(3)$ Kondo resonance in GNBs.

Conclusion and discussion.– The Kondo behavior found here is formed by zero-energy LSs with different flavors, in sharp contrast with the conventional Kondo effect arising from the vacancy-induced local moments in bipartite lattices [48, 58]. The key difference here is that the spin degrees of freedom are not involved in the screening process. Thus, the Kondo resonance peak here will not split even under extreme magnetic fields. Meanwhile, the Kondo cloud here, which is essentially a ‘‘flavor singlet’’, would be immune to measurements that probe spin or magnetic properties, such as the nuclear magnetic resonance spectroscopy. However, the transport anomalies, such as the resistivity minima, maintain to characterize the collective Fermi liquid behavior of the bath [59] at the strongly-coupling fixed point. The mechanism found here is not limited to graphene, but applicable to a wide class of 2D materials exhibiting nanobubbles and strain-induced quantization [60–62]. Last, we highlight that we have double verified the Kondo resonance via exact diagonalization, as presented in Supplemental Materials [47]. This confirms the emergent Kondo phenomena as an inherent property of GNBs.

GNBs have been recently demonstrated to be programmable [27]. Using functional atomic force microscopy (AFM), the size, shape, location and the number of GNBs can all be controlled [27]. This offers an unparalleled platform to

simulate various $SU(N)$ Kondo lattices with flexible configurations and tunable N . For example, aligning GNBs in 1D would realize an $SU(N_i)$ chain model with site-dependent N_i . In certain setups, exotic Kondo phenomena could be expected and even designed [47]. In addition, applying the gate voltage and displacement fields on bilayers can readily turn the Kondo resonance on-and-off. Therefore, the programmable GNBs could serve as promising lego-like building blocks to simulate exotic correlated phenomena beyond conventional heavy fermion systems.

R. W. acknowledges Shaochun Li, Jianpeng Liu, Wei Su for fruitful discussions. This work was supported by the National R&D Program of China (2022YFA1403601), the Innovation Program for Quantum Science and Technology (Grant no. 2021ZD0302800), the National Natural Science Foundation of China (No. 12322402, No. 12274206), and the Xiaomi foundation.

* rwang89@nju.edu.cn

† bgwang@nju.edu.cn

- [1] J. Kondo, *Prog. Theor. Phys.* **32**, 37 (1964).
- [2] K. G. Wilson, *Rev. Mod. Phys.* **47**, 773 (1975).
- [3] A. V. Balatsky, I. Vekhter, and J.-X. Zhu, *Rev. Mod. Phys.* **78**, 373 (2006).
- [4] Y. Meir, K. Hirose, and N. S. Wingreen, *Phys. Rev. Lett.* **89**, 196802 (2002).
- [5] M. Grobis, I. G. Rau, R. M. Potok, H. Shtrikman, and D. Goldhaber-Gordon, *Phys. Rev. Lett.* **100**, 246601 (2008).
- [6] B. Béri and N. R. Cooper, *Phys. Rev. Lett.* **109**, 156803 (2012).
- [7] A. C. Hewson, *The Kondo Problem to Heavy Fermions*, (Cambridge University Press, Cambridge, England, 1993).
- [8] S. M. Cronenwett, T. H. Oosterkamp, and L. P. Kouwenhoven, *Science* **281**, 540 (1998).
- [9] M. Pustilnik and L. Glazman, *J. Phys.: Condens. Matter* **16**, R513 (2004).
- [10] W. Liang, M. P. Shores, M. Bockrath, J. R. Long, and H. Park, *Nature* **417**, 725 (2002).
- [11] A. Carmi, Y. Oreg, and M. Berkooz, *Phys. Rev. Lett.* **106**, 106401 (2011).
- [12] P. Jarillo-Herrero, J. Kong, H. S. J. van der Zant, C. Dekker, L. P. Kouwenhoven, and S. De Franceschi, *Nature* **434**, 484 (2005).
- [13] A. Makarovski, A. Zhukov, J. Liu, and G. Finkelstein, *Phys. Rev. B* **75**, 241407(R) (2007).
- [14] T.-F. Fang, W. Zuo, and H.-G. Luo, *Phys. Rev. Lett.* **101**, 246805 (2008).
- [15] S. Sasaki, S. Amaha, N. Asakawa, M. Eto, and S. Tarucha, *Phys. Rev. Lett.* **93**, 017205 (2004).
- [16] W. Chen, Y. Yan, M. Ren, T. Zhang, and D. Feng, *Sci. China Phys. Mech. Astron.* **65**, 246811 (2022).
- [17] R. Zheng, R.-Q. He and Z.-Y. Lu, *Chinese Phys. Lett.* **35**, 067301 (2018).
- [18] G. Chen and J. L. Lado, *Phys. Rev. Research* **2**, 033466 (2020).
- [19] D. Ma, H. Chen, H. Liu, and X. C. Xie, *Phys. Rev. B* **97**, 045148 (2018).
- [20] C. Lacroix and M. Cyrot, *Phys. Rev. B* **20**, 1969 (1979).
- [21] H. Tsunetsugu, M. Sigrist, and K. Ueda, *Rev. Mod. Phys.* **69**, 809 (1997).
- [22] M. Tachiki and S. Maekawa, *Phys. Rev. B* **29**, 2497 (1984).
- [23] V. Alexandrov, P. Coleman, and O. Erten, *Phys. Rev. Lett.* **114**, 177202 (2015).
- [24] M. Dzero, K. Sun, V. Galitski, and P. Coleman, *Phys. Rev. Lett.* **104**, 106408 (2010).
- [25] Z. Dai, Y. Hou, D. A. Sanchez, G. Wang, C. J. Brennan, Z. Zhang, L. Liu, and N. Lu, *Phys. Rev. Lett.* **121**, 266101 (2018).
- [26] M. Settnes, S. R. Power, M. Brandbyge, and A.-P. Jauho, *Phys. Rev. Lett.* **117**, 276801 (2016).
- [27] P. Jia, W. Chen, J. Qiao, M. Zhang, X. Zheng, Z. Xue, R. Liang, C. Tian, L. He, Z. Di, and X. Wang, *Nat. Commun.* **10**, 3127 (2019).
- [28] J. Lu, A.H. C. Neto, and K. P. Loh, *Nat. Commun.* **3**, 823 (2012).
- [29] H. G.-Kalashami, K. S. Vasu, R. R. Nair, F. M. Peeters, and M. N.-Amal, *Nat. Commun.* **8**, 15844 (2017).
- [30] J. Ren, H. Guo, J. Pan, Y. Yang, Z. X. Wu, H.-G. Luo, S. Du, S. T. Pantelides, and H.-J. Gao, *Nano Lett.* **14**, 4011 (2014).
- [31] Y. Zhang, L. Li, J.-Hua Sun, D.-Hui Xu, R. Lü, H.-G. Luo, and W.-Q. Chen, *Phys. Rev. B* **101**, 035124 (2020).
- [32] L. Li, Y.-Y. Ni, Y. Zhong, T.-F. Fang and H.-G. Luo, *New J. Phys.* **15**, 053018 (2013).
- [33] H.-B. Zhuang, Q.-F. Sun and X. C. Xie, *Euro. Phys. Lett.* **86**, 58004 (2009).
- [34] S.-M. Choi, S.-H. Jhi, and Y.-W. Son, *Phys. Rev. B* **81**, 081407(R) (2010).
- [35] V. M. Pereira, A. H. Castro Neto, and N. M. R. Peres, *Phys. Rev. B* **80**, 045401 (2009).
- [36] F. de Juan, J. L. Mañes, and M. A. H. Vozmediano, *Phys. Rev. B* **87**, 165131 (2013).
- [37] N. Levy, S. A. Burke, K. L. Meaker, M. Panlasigui, A. Zettl, F. Guinea, A. H. Castro Neto, and M. F. Crommie, *Science* **329**, 544 (2010).
- [38] E. V. Castro, M. A. Cazalilla, and M. A. H. Vozmediano, *Phys. Rev. B* **96**, 241405(R) (2017).
- [39] S. Rachel, I. Göthel, D. P. Arovas, and M. Vojta, *Phys. Rev. Lett.* **117**, 266801 (2016).
- [40] Z. F. Ezawa, *Quantum Hall effects: Field theoretical approach and related topics* (World Scientific Publishing Company, 2008).
- [41] R. C. Bastos, M. Ochoa, S.A. Zavala, and F. Mireles, *Phys. Rev. B* **98**, 165436 (2018).
- [42] M. N. Amal, L. Covaci, K. Shakouri, and F. M. Peeters, *Phys. Rev. B* **88**, 115428 (2013).
- [43] V. M. Pereira, and A. H. Castro Neto, *Phys. Rev. Lett.* **103**, 046801 (2009).
- [44] L.-J. Yin, S.-Y. Li, J.-B. Qiao, J.-C. Nie, and L. He, *Phys. Rev. B* **91**, 115405 (2015).
- [45] R. Roldán, A. Castellanos-Gomez, E. Cappelluti, and F. Guinea, *J. Phys. Condens. Matter* **27**, 313201 (2015).
- [46] H. C. Park, J. Y. Han, and N. Myoung, *Quantum Sci. Technol.* **8**, 025012 (2023).
- [47] See supplemental materials for pertinent technical details on relevant proofs and derivations.
- [48] E. H. Lieb, *Phys. Rev. Lett.* **62**, 1201 (1989).
- [49] B. Sutherland, *Phys. Rev. B* **34**, 5208 (1986).
- [50] M. Inui, S. A. Trugman, and E. Abrahams, *Phys. Rev. B* **49**, 3190 (1994).
- [51] M. Schneider, D. Faria, S. Viola Kusminskiy, and N. Sandle, *Phys. Rev. B* **91**, 161407(R) (2015).
- [52] The Coulomb interaction becomes quite dominant in the GNB due to the presence of degenerate LSs. However, it can be omitted in the bath, because it merely leads to Fermi liquid corrections. Note that unlike the pristine bilayer graphene in thermodynamic limit, the bath $\bar{\Omega}$ does not possess quadratic band touching points at $E = 0$. Thus, the Coulomb interaction is irrelevant in the bath.

- [53] X.-F. Wang and T. Chakraborty, Phys. Rev. B **75**, 041404(R) (2007).
- [54] E. McCann and M. Koshino, Rep. Prog. Phys. **76**, 056503 (2013).
- [55] R. Wang, W. Su, J.-X. Zhu, C. S. Ting, H. Li, C. Chen, B. Wang, and X. Wang, Phys. Rev. Lett. **122**, 087001 (2019)
- [56] R. Žitko, Phys. Rev. B **81**, 241414(R) (2010).
- [57] R. Bulla, T. A. Costi, and T. Pruschke, Rev. Mod. Phys. **80**, 395 (2008).
- [58] J.-H. Chen, L. Li, W. G. Cullen, E. D. Williams and M. S. Fuhrer, Nat. Phys. **7**, 535 (2011).
- [59] C. Mora, Phys. Rev. B **80**, 125304 (2009).
- [60] M. Gastaldo, J. Varillas, Á. Rodríguez, M. Velický, O. Frank, and M. Kalbáč, npj 2D Mater. Appl. **7**, 71 (2023).
- [61] Y. Qi, M. A. Sadi, D. Hu, M. Zheng, Z. Wu, Y. Jiang, and Y. P. Chen, Adv. Mater. **35**, 2205714 (2023).
- [62] C. Zhao, M. Hu, J. Qin, B. Xia, C. Liu, S. Wang, *et al.*, Phys. Rev. Lett. **125**, 046801 (2020).
-

Supplemental material for: Programmable Kondo Effect Formed by Landau Levels

1. GAUSSIAN DEFORMATION

The in-plane lattice deformation in a GNB is caused by the out-of-plane (z-direction) lattice variation, which can be described by the Gaussian function,

$$z(\mathbf{r}) = h_0 e^{-r^2/2\sigma^2}, \quad (\text{S1})$$

where h_0 is the maximum deformation at the center of the bubble and σ characterizes the radius of the bubble. The strain tensor is obtained as

$$u_{xx} = \frac{h_0^2}{2\sigma^4} x^2 e^{-r^2/\sigma^2}, \quad u_{yy} = \frac{h_0^2}{2\sigma^4} y^2 e^{-r^2/\sigma^2}, \quad u_{xy} = \frac{h_0^2}{2\sigma^4} xy e^{-r^2/\sigma^2}. \quad (\text{S2})$$

The hopping t_n along the bond δ_n is then calculated using $t_n = t_0 e^{-\beta(|\mathbf{d}_n|/a-1)}$, where $\mathbf{d}_n = \delta_n + \bar{u}\delta_n$. The pseudo magnetic field is accordingly obtained as,

$$\mathbf{B} = \xi \frac{\beta}{a} \frac{h_0^2}{\sigma^6} e^{-r^2/\sigma^2} r^3 \sin(3\theta) \hat{z}, \quad (\text{S3})$$

where $\xi = \pm$ for the \mathbf{K} and \mathbf{K}' valley, respectively. In Fig.2(a) of the main text, we plot the hopping t_n throughout the 2D lattice. As shown, t_n becomes almost zero, i.e., $t_n \ll t_0$, at the boundary of GNB, $|\mathbf{r}| \sim \sigma$. Thus, the strained region in the GNB is automatically decoupled from the rest, unstrained area of the lattice. The decoupled GNB, denoted by Ω , is therefore described by

$$H_{\text{sys}} = - \sum_{\mathbf{r} \in \Omega, n} t_n \psi^\dagger(\mathbf{r}) \psi(\mathbf{r} + \delta_n) + \text{h.c.} \quad (\text{S4})$$

Eq.(S4) is a bipartite model on Ω with generally different (but close) site numbers on A and B sublattice, N_A and N_B . For $N = N_B - N_A \neq 0$ (assuming $N_B > N_A$), zero modes occur, whose degeneracy is $N_B - N_A$. For the strained graphene flake, the zero modes are attributed to the zeroth Landau level. The corresponding eigenstates of these zero modes are orthogonal to each other and are sublattice polarized. Specifically, they are polarized on B (A) for $N_B > N_A$ ($N_A > N_B$), as shown by Fig.2(c),(d) of the main text.

2. THE DENSITY OF STATES OF THE THERMAL BATH

For the AB-stacked bilayer graphene $H_{AB} = H_t + H_b + V$, where $H_{t/b}$ are the Hamiltonian of the top and bottom monolayer graphene, V represents for the coupling between them, which includes the coupling between the dimer and non-dimer sites [S1]. We denote the strained GNB on the top layer as the subsystem Ω , and the rest as the thermal bath $\bar{\Omega}$. The total system can be rewritten as,

$$H_{AB} = H_{\text{sys}} + H_{\text{bath}} + H_{\text{coup}}, \quad (\text{S5})$$

where H_{bath} represents the strain-free bilayer subtracted by Ω , and H_{coup} denotes the coupling between them.

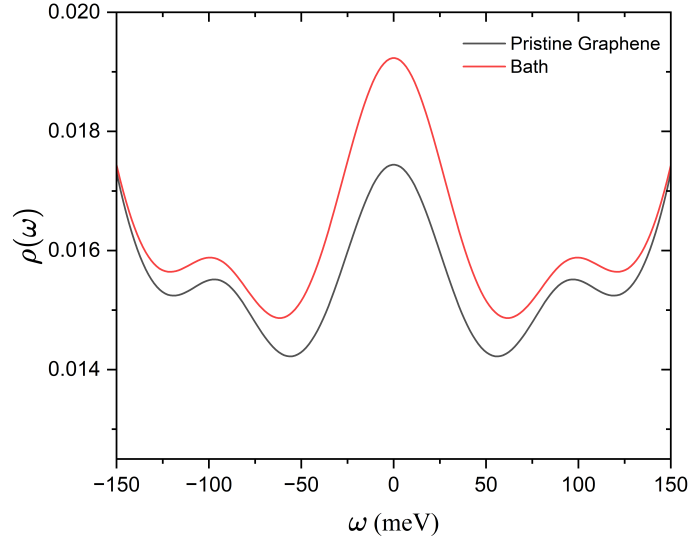


FIG. S1. Comparison between the DOS of the pristine graphene bilayer and the bath in the low-energy window.

We calculate and compare in details the density of states (DOS) of the bath and that of the pristine graphene bilayer. As shown by Fig.S1 the DOS resemble each other even in the zoomin low-energy window.

3. EFFECTIVE $SU(N)$ KONDO MODEL

3.1 Landau wave functions and flavor quantum number

The zero modes in the GNB can be understood as Landau orbits generated by the pseudo magnetic field. For the triaxial strain case, the Landau wavefunction can be obtained analytically under the uniform pseudomagnetic field. For relatively large GNB, the subsystem Ω exhibits the low-energy theory as that of the monolayer graphene, i.e.,

$$H_{\text{sys}} = v_F \sum_{\mathbf{k}, \xi=\pm} \psi_{\mathbf{k}}^{(\xi)\dagger} \boldsymbol{\sigma}^{(\xi)} \cdot \mathbf{k} \psi_{\mathbf{k}}^{(\xi)}, \quad (\text{S6})$$

where $\xi = \pm$ denotes the two valleys K^+ , K^- , and $\boldsymbol{\sigma}^{(\pm)} = (\sigma_x, \pm\sigma_y)$. Under pseudomagnetic field induced by the triaxial strain, the momentum in Eq.(S6) is cast into $\mathbf{k} = -i\nabla \rightarrow -i\nabla + \mathbf{A}$, and $\mathbf{A} = (A_x, A_y)$. Since the two valleys are decoupled, the Landau wave function can be solved independently for each valley. For K^+ , the eigen-equation to be solved is

$$(-i\nabla + \mathbf{A}) \cdot \boldsymbol{\sigma}^{(+)} \Psi_n^{(+)}(\mathbf{r}) = E_n \Psi_n^{(+)}(\mathbf{r}), \quad (\text{S7})$$

where v_F is set to 1. The eigen-equation for the K^- valley is similar and thus not written explicitly. $\Psi_n^{(\xi)}(\mathbf{r}) = [\phi_{n,A}^{(\xi)}(\mathbf{r}), \phi_{n,B}^{(\xi)}(\mathbf{r})]^T$ with being n the index of Landau levels is the Landau wave function for valley ξ on the A and B sublattice.

We focus on the lowest Landau level $n = 0$ and on solving the zero energy eigen-equation by setting $E_0 = 0$. In the following, we neglect the $n = 0$ index for brevity, and we adopt the symmetric gauge $A_x = -By/2$ and $A_y = Bx/2$. The general solution is obtained for $B > 0$ as

$$\phi_B^{(+)}(\mathbf{r}) = f_B^{(+)}(\mathbf{r}) e^{-\lambda(\mathbf{r})}, \quad (\text{S8})$$

$$\phi_A^{(+)}(\mathbf{r}) = 0, \quad (\text{S9})$$

where

$$\lambda(\mathbf{r}) = \frac{B}{2\pi} \int d\mathbf{r}' \ln(|\mathbf{r} - \mathbf{r}'|/r_0), \quad (\text{S10})$$

with r_0 being a constant which can be later absorbed into the normalization factor. The asymptotic solution for large $r = |\mathbf{r}| \gg$

r_0 is further simplified into,

$$\phi_B^{(+)}(\mathbf{r}) = (r/r_0)^{-\frac{\Phi}{2\pi}} f_B^{(+)}(\mathbf{r}), \quad (\text{S11})$$

$$\phi_A^{(+)}(\mathbf{r}) = 0, \quad (\text{S12})$$

where $\Phi = BA$ with A being the area is the total flux through the system Ω , and $f_B^{(+)}$ satisfies,

$$-\partial_{\bar{z}} f_B^{(+)} = 0, \quad (\text{S13})$$

where the complex coordinate $z = y + ix$ is introduced. The general solution to Eq.(S13) is

$$f_B^{(+)} = \sum_{m=0}^{\infty} a_m z^m, \quad (\text{S14})$$

where a_m is the normalization factor. Insertion of Eq.(S14) into $\phi_B^{(+)}(\mathbf{r})$ leads to

$$\phi_B^{(+)}(\mathbf{r}) = \sum_{m=0}^{N_\Phi} a_m z^m (r/r_0)^{-\Phi/2\pi} = \sum_{m=0}^{\tilde{N}} a_m \phi_{B,m}^{(+)}(\mathbf{r}), \quad (\text{S15})$$

where $N_\Phi = [\Phi/2\pi]$ denotes the largest integer part of $\Phi/2\pi$, i.e., the number of flux quanta. Note that any physical solutions in Eq.(S15) must be normalizable. This sets an upper bound in the sum of m , i.e., $m \leq N_\Phi$. Thus, the solution for large r is analytically obtained as

$$\psi^{(+)}(\mathbf{r}) = \sum_{m=0}^{N_\Phi} a_m \Psi_m^{(+)}, \quad (\text{S16})$$

$$(\text{S17})$$

where

$$\Psi_m^{(+)} = [0, z^m (r/r_0)^{-\Phi/2\pi}]^T. \quad (\text{S18})$$

Thus, there are $N_\Phi + 1$ degenerate states, $\Psi_m^{(+)}$, in the zeroth Landau level with $E_0 = 0$, characterized by the quantum number m , which is the orbital angular momentum (OAM). The full solutions covering $r < r_0$ can be found by evaluating Eq.(S10). The results for K^- valley can also be similarly derived.

For finite sized nanobubbles, the geometry effect would slightly violate the valley symmetry and results in difference between the number of degenerate states in the two valleys. Thus, $N_\Phi^{(\pm)}$ should be separately introduced for each valley, which satisfy,

$$N_\Phi^{(+)} + N_\Phi^{(-)} + 2 = N = N_B - N_A. \quad (\text{S19})$$

For the simplest case with $N_B - N_A = 2$, $N_\Phi^{(+)} = N_\Phi^{(-)} = 0$, therefore only the $m = 0$ Landau orbit is present for each of the two valleys. Now it becomes clear that the N zero modes lie in a space expanded by the direct sum of the OAM (\mathbf{L}) in each valley ($\xi = \pm$), i.e., $\mathbb{L}_+ \oplus \mathbb{L}_-$, and these zero modes can be indexed by $j \equiv (m, \xi)$, i.e., $|j\rangle = |\Psi_m^{(\xi)}\rangle$.

The Landau sites have a convenient representation in the second quantized form. Here, we restore the Landau level index n and consider a generic electronic wave function $\psi(\mathbf{r}) = \langle \mathbf{r} | \psi \rangle$. Inserting the orthonormal completeness condition, $\sum_{n,j} |n, j\rangle \langle n, j| = 1$, we obtain $\psi(\mathbf{r}) = \sum_{n,j} \langle \mathbf{r} | n, j \rangle \langle n, j | \psi \rangle = \sum_{n,j} \Psi_{n,j}(\mathbf{r}) d_{n,j}$, where $\Psi_{n,j}(\mathbf{r})$ is the wavefunction for Landau sites j in the n -th Landau level, and $d_{n,j}$ is defined by

$$d_{n,j} = \langle n, j | \psi \rangle = \int d\mathbf{r} \langle n, j | \mathbf{r} \rangle \langle \mathbf{r} | \psi \rangle = \int d\mathbf{r} \Psi_{n,j}^*(\mathbf{r}) \psi(\mathbf{r}). \quad (\text{S20})$$

After promoting $\psi(\mathbf{r})$ to field operator $\hat{\psi}(\mathbf{r})$ in Eq.(S20), $d_{n,j}$ is accordingly promoted to the fermionic operator, which satisfies the anticommutative relation,

$$\{d_{n,j}, d_{n',j'}^\dagger\} = \delta_{nn'} \delta_{jj'}. \quad (\text{S21})$$

d_{nj}^\dagger creates the Landau site $|n, j\rangle$ on top of the vacuum, i.e., $|n, j\rangle = d_{n,j}^\dagger |0\rangle$. In the following, we focus on the zero modes on the zeroth Landau level, thus only the Landau site operators, d_j and d_j^\dagger are relevant, where $n = 0$ is implicit.

3.2 Conservation of the flavor quantum number

We now consider the system-bath hybridization. As shown by Fig.1 above, the DOS of the bath is qualitatively comparable to that of the pristine bilayer graphene. Since it is well known that the Kondo resonance, if exists, is determined by the bath DOS around the Fermi energy, one can safely replace the bath by an pristine graphene bilayer to study the Kondo behavior. The bath is therefore described by

$$H_{\text{bath}} = \sum_{\mathbf{k}, \xi} \psi_{\mathbf{k}}^{(\xi)\dagger} \mathcal{H}_{\text{bath}}^{(\xi)}(\mathbf{k}) \psi_{\mathbf{k}}^{(\xi)}, \quad (\text{S22})$$

where

$$\mathcal{H}_{\text{bath}}^{(\pm)}(\mathbf{k}) = -\frac{1}{2m} \begin{pmatrix} 0 & (\pi_{\mathbf{k}}^{(\pm)\dagger})^2 \\ (\pi_{\mathbf{k}}^{(\pm)})^2 & 0 \end{pmatrix}, \quad (\text{S23})$$

where $\pi_{\mathbf{k}}^{(\pm)} = \pm k_x + ik_y$.

For the purpose of brevity, we introduce the ket state to denote the sublattice basis, i.e., $|\psi_{\mathbf{k}}^{(\xi)}\rangle = [|\phi_{\mathbf{k},A}^{(\xi)}\rangle, |\phi_{\mathbf{k},B}^{(\xi)}\rangle]^T$ for ξ valley. The Hamiltonian in Eq.(S23) can be diagonalized by a unitary transformation, i.e.,

$$U^\dagger \mathcal{H}_{\text{bath}}^{(\pm)}(\mathbf{k}) U = \epsilon_k \sigma_z, \quad (\text{S24})$$

where $\epsilon_k = k^2/2m$, and

$$U^{(\pm)} = \frac{1}{\sqrt{2}} \begin{pmatrix} 1 & 1 \\ -e^{\pm 2i\theta} & e^{\pm 2i\theta} \end{pmatrix}, \quad (\text{S25})$$

and θ is the angle of \mathbf{k} (or equivalently the angle of \mathbf{r}). Meanwhile, the basis is changed to $|c_{\mathbf{k}}^{(\xi)}\rangle = U^{(\xi)\dagger} |\psi_{\mathbf{k}}^{(\xi)}\rangle = [|c_{\mathbf{k},+}^{(\xi)}\rangle, |c_{\mathbf{k},-}^{(\xi)}\rangle]^T$, where “ \pm ” denotes the conduction and valence bands.

We need to evaluate the hybridization between the Landau site $|j\rangle$ and the bath states. Note that the Landau site $|j\rangle$ (Eq.(S18)) has zero component on A sublattice, thus only the overlap with $|\phi_{\mathbf{k},B}^{(\xi)}\rangle$ is non-vanishing. We have $|\phi_{\mathbf{k},B}^{(\xi)}\rangle = (-e^{i2\xi\theta} |c_{\mathbf{k},-}^{(\xi)}\rangle + e^{i2\xi\theta} |c_{\mathbf{k},+}^{(\xi)}\rangle) / \sqrt{2}$, and the hybridization reads $V = \langle j | \phi_{\mathbf{k},B}^{(\xi')} \rangle = \langle \phi_{B,m}^{(\xi)} | \phi_{\mathbf{k},B}^{(\xi')} \rangle$, where $\langle \phi_{B,m}^{(\xi)} |$ denotes the bra state corresponding to wavefunction $\phi_{B,m}^{(\xi)}(\mathbf{r})$ in Eq.(S15). Then, we obtain

$$V = \langle \phi_{B,m}^{(\xi)} | \phi_{\mathbf{k},B}^{(\xi')} \rangle = \frac{1}{\sqrt{2}} e^{i2\xi\theta} \delta_{\xi\xi'} [-\langle \phi_{B,m}^{(\xi)} | c_{\mathbf{k},+}^{(\xi)} \rangle + \langle \phi_{B,m}^{(\xi)} | c_{\mathbf{k},-}^{(\xi)} \rangle] = V_+ + V_-, \quad (\text{S26})$$

where V_{\pm} denotes the hybridization between the Landau sites and the bath electrons of the conduction/valence band. It is obtained that

$$\begin{aligned} V_+ &= -\frac{1}{\sqrt{2}} \delta_{\xi\xi'} \int d\mathbf{r} e^{2i\xi\theta} \langle \phi_{B,m}^{(\xi)} | \mathbf{r} \rangle \langle \mathbf{r} | c_{\mathbf{k},+}^{(\xi)} \rangle = -\frac{1}{\sqrt{2}} \delta_{\xi\xi'} \sum_{m'} \int dr r \int d\theta e^{2i\xi\theta} \phi_{B,m}^{(\xi)*}(\mathbf{r}) \langle r | c_{k,m',+}^{(\xi)} \rangle e^{im'\theta} \\ &= -\frac{1}{\sqrt{2}} \delta_{\xi\xi'} \sum_{m'} \int dr r \int d\theta e^{2i\xi\theta} \phi_{B,m}^{(\xi)*}(\mathbf{r}) u_{k,m',+}(r) e^{im'\theta}, \end{aligned} \quad (\text{S27})$$

where we have represented the Bloch state of the bath by the OAM partial waves, i.e., $u_{\mathbf{k},+}^{(\xi)}(\mathbf{r}) = \langle \mathbf{r} | c_{\mathbf{k},+}^{(\xi)} \rangle = \sum_{m'} \langle r | c_{k,m',+}^{(\xi)} \rangle e^{im'\theta} = \sum_{m'} u_{k,m',+}(r) e^{im'\theta}$, in which \mathbf{r} can be fixed along the x direction since it is the angle between \mathbf{k} and \mathbf{r} that matters. Insertion of $\phi_{B,m}^{(\xi)*}(\mathbf{r})$ in Eq.(S15) to Eq.(S27) leads to

$$V_+ = -\frac{1}{\sqrt{2}} \sum_{m'} \delta_{\xi\xi'} \delta_{m',m\xi-2\xi} u_{k,\xi,m'} \quad (\text{S28})$$

where we defined $v_{k,\xi,m} = \int dr r r^m (r/r_0)^{-\Phi/2\pi} u_{k,m,\pm}^{(\xi)}(r)$, which is an overlap between the radial components of the Bloch state and the Landau site. Note that amplitude $v_{k,\xi,m'}$ is the same for both the hybridization to the conduction and valence band.

Similarly, V_- is obtained as,

$$V_- = \frac{1}{\sqrt{2}} \sum_{m'} \delta_{\xi\xi'} \delta_{m',m\xi-2\xi} v_{k,\xi,m'} \quad (\text{S29})$$

The two delta functions here, $\delta_{\xi\xi'}$ and $\delta_{m',m\xi-2\xi}$, clearly demonstrate the flavor conservation, i.e., $j = (m, \xi)$.

In second-quantized form, the single-particle hybridization in Eq.(S28) and Eq.(S29) is cast into,

$$H_{\text{hyb}} = \int dk \sum_{m,\xi} d_{m,\xi}^\dagger v_{k,\xi,m\xi-2\xi} (-c_{k,m\xi-2\xi,+} + c_{k,m\xi-2\xi,-}) + h.c. \quad (\text{S30})$$

To make the form more concise, we define fermionic operators $\tilde{c}_{k,j,\pm} = c_{k,m\xi-2\xi,\pm}$, and

$$H_{\text{hyb}} = \int dk \sum_j v_{k,j} d_j^\dagger (-\tilde{c}_{k,j,+} + \tilde{c}_{k,j,-}) + h.c. \quad (\text{S31})$$

The hybridization of the Landau sites to the bath is thus fully captured by the coupling to an effective fermions (with 1D wave vector), in which the flavor j is conserved.

Last, the bath Hamiltonian H_{bath} can be transformed accordingly, first to the diagonal band basis under the unitary transformation and then to the OAM space, leading to

$$\begin{aligned} H_{\text{bath}} &= \int dk \sum_{n,m} \epsilon_{k,n} c_{k,m,n}^{(+)\dagger} c_{k,m,n}^{(+)} + \int dk \sum_{n,m} \epsilon_{k,n} c_{k,m,n}^{(-)\dagger} c_{k,m,n}^{(-)} \\ &= \int dk \sum_{n,m} \epsilon_{k,n} c_{k,m-2,n}^{(+)\dagger} c_{k,m-2,n}^{(+)} + \int dk \sum_{n,m} \epsilon_{k,n} c_{k,-m+2,n}^{(-)\dagger} c_{k,-m+2,n}^{(-)} \\ &= \int dk \sum_{n,j} \epsilon_{k,n} \tilde{c}_{k,j,n}^\dagger \tilde{c}_{k,j,n}, \end{aligned} \quad (\text{S32})$$

where $\epsilon_{k,n} = nk^2/2m$, with the band index $n = \pm$.

3.3 $SU(N)$ Anderson model and NRG calculations

The Landau sites have completely quenched kinetic energies and are described by

$$H_d = \sum_{j=1}^N \epsilon_d d_j^\dagger d_j, \quad (\text{S33})$$

where $N = N_B - N_A$, and $\epsilon_d = 0$ as the Landau sites are zero modes. In addition, the repulsive interaction between electrons is non-negligible in the nanobubble. We consider the general repulsive interaction $H_{\text{int}} = \int d\mathbf{r} d\mathbf{r}' U(\mathbf{r} - \mathbf{r}') \psi^\dagger(\mathbf{r}) \psi(\mathbf{r}) \psi^\dagger(\mathbf{r}') \psi(\mathbf{r}')$. Projection of the interaction H_{int} to the zeroth Landau level $n = 0$ leads to [S2]:

$$H_{\text{int}} = \sum_{ijpq} U_{ijpq} d_i^\dagger d_p^\dagger d_q d_j, \quad (\text{S34})$$

where the conservation law $i + j = p + q$ is implied, and U_{ijpq} reads,

$$U_{ijpq} = \frac{1}{4\pi} \int d\mathbf{q} U_D(\mathbf{q}) \langle i | e^{i\mathbf{q}\cdot\mathbf{X}} | j \rangle \langle p | e^{-i\mathbf{q}\cdot\mathbf{X}} | q \rangle, \quad (\text{S35})$$

where \mathbf{X} is the guiding center coordinate, $U_D(\mathbf{q}) = U(\mathbf{q})e^{-q^2 l_B^2/2}$ is the projected repulsive potential dressed by the zeroth Landau-level form factor. The direct integral can be extracted from Eq.(S34) as [S2]

$$H_U = \sum_{i \neq j} U_{iipp} d_i^\dagger d_i d_p^\dagger d_p \equiv \sum_{i \neq j} U_{ij} n_{d,i} n_{d,j}, \quad (\text{S36})$$

where $n_{d,i} = d_i^\dagger d_i$. As will be clear in the following, with taking into account the hybridization to the bath, the direct integral is the most relevant term, which leads to a Kondo exchange interaction flowing to the strongly-coupling fixed point. The other interaction channels do not affect the Kondo fixed point, as is verified by the exact diagonalization calculation in Sec. 6.

Collecting Eq.(S33) and Eq.(S36), we obtain the Hamiltonian of the interacting Landau sites,

$$H_{\text{imp}} = \sum_{j=1}^N \epsilon_d d_j^\dagger d_j + \sum_{i \neq j} U_{ij} n_{d,i} n_{d,j}. \quad (\text{S37})$$

Eq.(S37), Eq.(S32) and Eq.(S31) altogether are in close analogy of an Anderson impurity model, where the impurity has $SU(N)$ symmetry and is coupled to an effective 1D bath with 1D momentum k . Following Ref.[S3], we further define the following fermionic operators that mix the two bands, i.e.,

$$\gamma_{\epsilon,j} = [-\tilde{c}_{\epsilon,j,+} \theta(\epsilon) + \tilde{c}_{\epsilon,j,-} \theta(-\epsilon)]/2 \quad (\text{S38})$$

$$\gamma_{\epsilon,j}^\dagger = [-\tilde{c}_{\epsilon,j,+}^\dagger \theta(\epsilon) + \tilde{c}_{\epsilon,j,-}^\dagger \theta(-\epsilon)]/2, \quad (\text{S39})$$

where $\theta(x)$ is the Heaviside step function. Then, in the energy representation [S4], H_{bath} and H_{hyb} in Eq.(S32) and Eq.(S31) are transformed to,

$$H_{\text{bath}} = \sum_{j=1}^N \int d\epsilon (\epsilon - \mu) \gamma_{\epsilon,j}^\dagger \gamma_{\epsilon,j}, \quad (\text{S40})$$

and

$$H_{\text{hyb}} = \sum_{j=1}^N \int d\epsilon [h_j(\epsilon) d_j^\dagger \gamma_{\epsilon,j} + h.c.]. \quad (\text{S41})$$

where a chemical potential of the bath μ is introduced, which can be modulated by gate voltage. Here, for the case $v_{j,k}$ being independent of k , $h_j^2(\epsilon) = v_j^2 \rho_{\bar{\Omega}}(\epsilon)$ is the familiar broadening function with $\rho_{\bar{\Omega}}(\epsilon)$ being DOS of the bath $\bar{\Omega}$. Since $\rho_{\bar{\Omega}}(\epsilon)$ is non-vanishing even for $E = 0$ (Fig.1 above), there is no pseudogap feature in the broadening function. In this case, the Kondo fixed point is known to be determined by the bath DOS near the Fermi energy [S5], i.e., $\rho(\mu)$.

4. DETAILS IN NRG CALCULATIONS

We consider two cases for example, i.e., $SU(2)$ and $SU(3)$ impurity model and perform NRG calculations. For a hardcore repulsion, evaluation of Eq.(S35) leads to

$$U_{ij} = U_{(\xi,m),(\xi',m')} = \frac{1}{8\pi l_B} \frac{(m+m')!}{2^{m+m'} m! m'}, \quad (\text{S42})$$

we set the smallest element in U_{ij} to be 40meV. For the $SU(2)$ case, the only interaction is $U_{(+,0),(-,0)}$. For the $SU(3)$ case, we have three components, $U_{(+,0),(-,0)}$, $U_{(+,1),(-,0)}$, $U_{(+,1),(+,0)}$. We define $U_1 = U_{(+,1),(-,0)} = U_{(+,1),(+,0)}$ and $U_2 = U_{(+,0),(-,0)}$. The chemical potential or the Fermi energy in Eq.(S40) ranges from ϵ_d to $\epsilon_d + U_1 + U_2$. $h_j(\epsilon)$ can be chosen to be a constant independent of j for simplicity [S5], i.e., $\Gamma = \pi h_j \rho(\mu)$ is a constant.

We study the mapped Anderson model by the full-density-matrix (FDM) NRG. The density of states of the non-interacting bath is taken as a constant, $\rho(\epsilon) = \rho_0 = 0.01$, within the interval $\epsilon \in [-D, D]$ and $D = 1$. The bath is discretized logarithmically and mapped to a semi-infinite Wilson chain with exponentially decaying hoppings, and the hybridization is mapped to the hopping between the impurity and the first chain site. The Coulomb interaction on the impurity site takes its value $U = 10\pi\rho_0$. The chain is diagonalized iteratively while discarding high-energy states, thereby gradually flowing to the low-energy window. The finite-size level spacing of a chain ending at site n has the energy of order $\omega_n \propto \Lambda^{(-n/2)}$. Here $\Lambda > 1$ is the logarithmical

discretization parameter and chosen to be 2 in the calculations. The FDM NRG is implemented with the symmetric tensors. The number of kept states used in the truncation is 1500. We calculate the temperature-dependent impurity thermodynamic quantities and the zero temperature impurity spectral function, as shown by Fig.4 of the main text. The impurity spectral function $\mathcal{A}(\omega)$ is broadened with a logarithmic gaussian function with a parameter $b = 0.8$, i.e.,

$$\delta(\omega - E) \rightarrow \frac{e^{-b^2/4}}{bE\sqrt{\pi}} e^{-[\ln(\omega/E)/b]^2}.$$

5. POSSIBLE EXTENSIONS TO EXPLORE NOVEL KONDO PHYSICS

The GNBs can be well manipulated by experiments, using techniques such as functional atomic force microscopy (AFM). The number, location, shape, and size of the GNBs can all be controlled, providing a versatile platform to explore correlated phenomena in Kondo lattices. Here, we discuss several interesting extensions that may stimulate further research.

First, by controlling the size of the GNB, N can be tuned successively, rendering possible the observation of the Kondo crossover from small to large N . We mention that the large N approximation is a standard approach in the study of heavy fermion systems, however its validity at small N needs to be verified. Our proposed GNB system therefore offers a feasible way to keep track of the evolution of the underlying physics with changing N .

Second, using the programmable GNBs, exotic Kondo lattice systems that are previously unfeasible can now be realized. For example, aligning the GNBs with small N to the left in a 1D chain and those with large N to the right, a “domain wall” may be created. It is interesting to investigate the property of the domain wall. For another example, one may expect realization of certain 1D “superlattices” of $SU(N)$ GNBs, such as an alternating $SU(2)$ - $SU(3)$ 1D Kondo lattice model. All these new structures may promise new Kondo phenomena beyond our existing knowledge.

Third, it is also interesting to investigate the graphene with nanobubbles, in proximity with superconducting materials. This offers a highly tunable platform to investigate $SU(N)$ Kondo phenomena in superconducting bath, which would host novel impurity physics beyond the conventional Yu-Shiba-Rusinov states.

6. EXACT DIAGONALIZATION VERIFICATION

To clearly confirm the above results, which are obtained from the effective theory of LSs in hybridization with the bath, we perform exact diagonalization (ED) calculations of tight-binding models on finite sized structures. We consider the simplest GNB, which constitutes a simplex with three B sites and one A site, as shown by Fig.S2. To verify the results, we consider two tight-binding models, respectively describing the GNB on a monolayer Fig.S2(a) and on a bilayer Fig.S2(b).

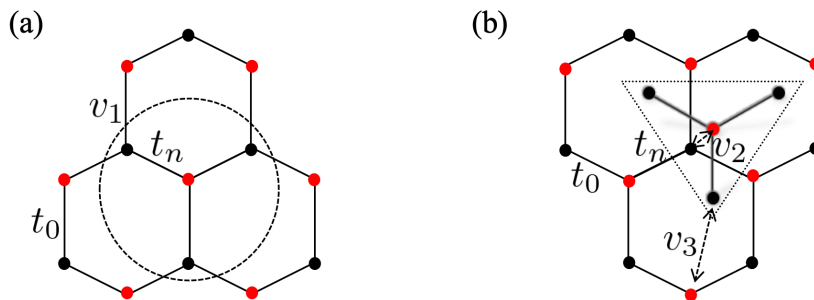


FIG. S2. Illustration of the models used the ED calculations. (a) The intra-layer model. The graphene nanobubble is a 4 sites simplex highlighted by the black dashed circle. The three bonds t_n GNB are modified by strain. v_1 is the intra-layer coupling strength between the GNB simplex and the rest of the sites. (b). The inter-layer model. The GNB simplex with strained bonds are Bernal-stacked on the unstrained bottom layer. v_2 and v_3 denote the γ_1 hopping and t_3 hopping, respectively.

For both models in Fig.2, the free Hamiltonian of the total system can be written as,

$$H_0 = - \sum_j t_j a_0^\dagger b_j + h.c. + V + H_{\text{bath}}, \quad (\text{S43})$$

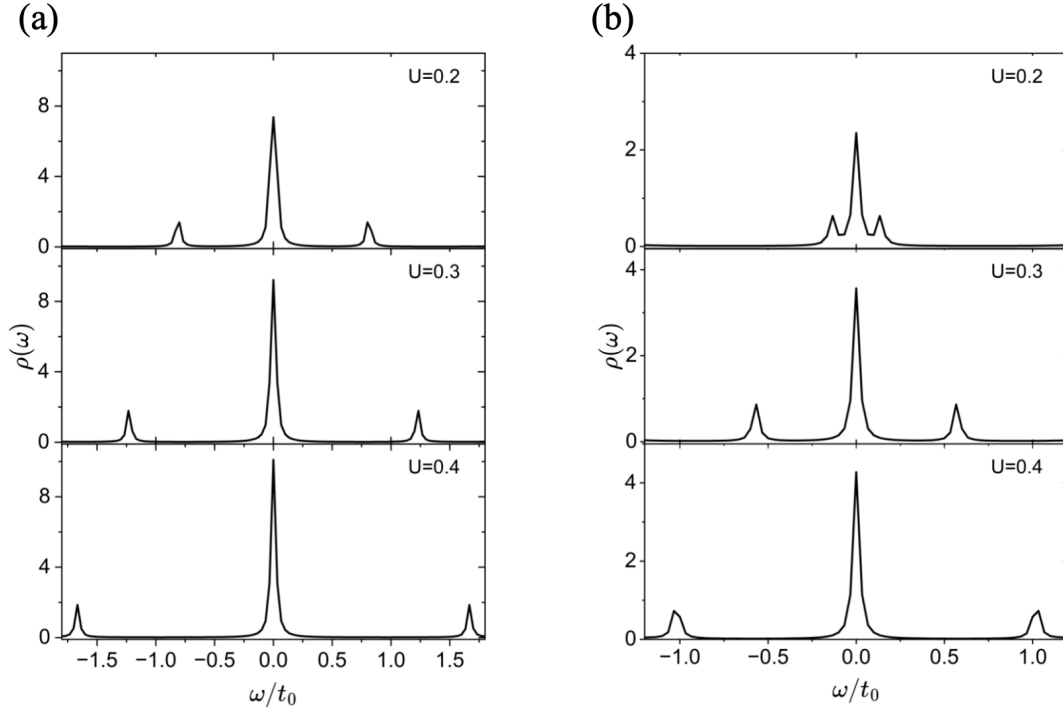


FIG. S3. Calculated LDOS of the GNB corresponding to two different models. (a). Results for the intra-layer mode with varying the nearest neighbor interaction U . The total system has 4 GNB sites and 9 bath sites. (b). Results for the inter-layer model with varying U . The total system has 4 GNB sites and 13 bath sites. In the ED calculations, the particle number conservation is utilized, with the electron number $N_e = 10$ in (a) and $N_e = 14$ in (b). In both models, the hopping parameter on the simplex is chosen as $t_n = 0.8t_0$. The other parameters are $v_1 = 0.1t_0$, $v_2 = 0.1\gamma_1$, and $v_3 = 0.1t_3$, where t_0 , γ_1 and t_3 represent the nearest neighbor hopping, dimer site hopping and non-dimer site hopping respectively in the pristine situation.

where the first term describes the GNB simplex, in which $j = 1, 2, 3$ denotes the three B sites, H_{bath} describes the rest of the sites. We denote the GNB sites as 0 to 3, and the bath sites to be $4 \dots L$, where $L + 1$ is the total size of the model. For both structures in Fig.S2(a) and Fig.S2(b), the coupling V is generally of the following form,

$$V = v_1 \sum_{j=1, \langle jk \rangle}^3 b_j^\dagger a_k + v_2 a_0^\dagger b_{k_0} + v_3 \sum_{j=1, \langle jk \rangle}^3 b_j^\dagger a_k + h.c. \quad (\text{S44})$$

For the intralayer model, $v_1 \neq 0$ and $v_2 = v_3 = 0$, while for the interlayer model, $v_1 = 0$ and $v_2 = v_3 \neq 0$. The intralayer v_1 term involves the coupling of the three B sites in the GNB to the nearest neighbor A sites in the bath. The interlayer terms v_2 and v_3 are respectively the hybridization of the dimer sites and the non-dimer sites, as shown by Fig.S2(b). $v_i < t_0$ with $i = 1, 2, 3$ are treated as parameters in the ED calculations.

We further take into account the short-range (nearest neighbor) density-density repulsive interaction U . Then, we perform ED calculation to obtain the energy spectra and then evaluate the LDOS in the strained GNB region. Denoting the energy spectra and the corresponding many-body eigenstates as $|m\rangle$ and E_m , the Green's function of the GNB can be obtained in the Lehmann representation as,

$$G_{ij}(\omega) = \sum_m \frac{\langle 0 | \psi_i | m \rangle \langle m | \psi_j^\dagger | 0 \rangle}{\omega^+ - (E_m - E_0)} + \sum_m \frac{\langle 0 | \psi_j^\dagger | m \rangle \langle m | \psi_i | 0 \rangle}{\omega^+ - (E_0 - E_m)}, \quad (\text{S45})$$

where $|0\rangle$ and E_0 denote the ground state and ground state energy, respectively, and ψ_i, ψ_i^\dagger are the annihilation and creation operators at site i of the GNB region. Then, the LDOS of the system can be evaluated by:

$$\rho(\omega) = -\frac{1}{\pi} \text{Im Tr } G(\omega + i0^+). \quad (\text{S46})$$

The DOS of the GNB is shown by Fig.S3. For both the intralayer and interlayer model, the significant LDOS peak at $\omega = 0$ is clearly obtained, in well agreement with our NRG calculations in the main text.

* rwang89@nju.edu.cn

† bgwang@nju.edu.cn

[S1] A. V. Rozhkov, A. O. Sboychakov, A. L. Rakhmanov, and F. Nori, Phys. Rep. **648**, 1 (2016).

[S2] Z.F. Ezawa, Quantum Hall Effects: Field Theoretical Approach and Related Topics, Peking University Press (2012).

[S3] R. Wang, W. Su, J.-X. Zhu, C. S. Ting, C. Chen, B. Wang, and X. Wang, Phys. Rev. Lett. **122**, 087001 (2019).

[S4] R. Žitko, Phys. Rev. B **81**, 241414(R) (2010).

[S5] R. Bulla, T. A. Costi, and T. Pruschke, Rev. Mod. Phys. **80**, 395 (2008).